15

Microwave Resonant Spectroscopy of Semiconductors with Micrometer Resolution

© A.N. Reznik, N.V. Vostokov

Institute of Physics of Microstructures, Russian Academy of Sciences,
603950 Nizhny Novgorod, Russia
e-mail: reznik@ipm.sci-nnov.ru

Received September 21, 2021
Revised December 6, 2021
Accepted December 7, 2021

We have proposed and experimentally verified a local method of microwave resonant spectroscopy of semiconductors. The microwave circuit of the spectrometer based on the Cascade Microtech probe station is equipped with a coaxial resonator of special geometry. As result, the measurement accuracy of the previously developed volt-impedance spectroscopy method was greatly increased. A technique for spectrometer calibration and resonant measurements of the complex impedance of the probe-sample system has been developed. We have measured the impedance of test structures with Schottky contacts of $30-60\,\mu$m in diameter on a single-crystal GaAs wafer at several discrete frequencies in the range of $50-250$ MHz. The nontrivial resistive properties of the structures are studied, which consist of the excess resistance that is $1-2$ orders higher than the spreading resistance for the alternating current in the unperturbed region of the semiconductor. The discovered effect is presumably associated with the a.c. charge modulation on deep levels of the semiconductor. A model calculation of the impedance spectrum has been performed, which demonstrates a good agreement with the experimental spectra.

Keywords: Microwave microscope, near field, probe, resonator, impedance, semiconductor.

DOI: 10.21883/JTF.2022.03.52145.262-21

Introduction

Electromagnet diagnostics — is an efficient tool for study of electrophysical characteristics of semiconductor materials and structures. However, obtainment of quantitative information on the scales below $100\,\mu$m still remains a quite serious problem. Infrared or optical diagnostics [1] is not enough informative with regard to the conducting properties, since the plasma frequency for semiconductors falls within the THz-range, which is poorly covered by the measurement instrumentation until now. Moreover, interpretation of the optical spectra of reflection and transmission coefficients is complicated by interzone absorption, availability of impurity lines and phonon mods. Additional challenges for semiconductor structures occur due to reflections on interfaces. Application of radio waves [2] fails to provide the required resolution even for millimeter waves due to fundamental limitation by the Rayleigh criterion. A unique (virtually unlimited) possibility of local measurements has appeared due to the development for the last 30 years of the method of near field microwave microscopy (NFMM). For such equipment the resolution is not limited to the wavelength, but it is determined by the probe aperture size. The devices of a low-frequency part of the radio range ($f < 50$ MHz) have not enough impedance sensitivity, because in the scales below $10-100\,\mu$m it is needed to measure the capacitance $C < 1$ fF. Preferred one is the microwave (MW) range, because the capacity impedance of the probe $Z = -j/(2\pi f C)$ is decreased as far as the frequency is growing. The MW microscopes sensitivity in terms of capacitance reach 1 aF [3]. It is already in the beginning of the period of fast growth of NFMM studies (the first half of 90-s) the resolution of the devices had achieved ~ 100 nm [4]. The first commercial microscope with the resolution of $3-5\,\mu$m is described in [5]. The resolution power of modern commercial microscopes (Agilent/Keysight, PrimeNano) reach $30-50$ nm due to adaptation of the probes of atomic-force microscopy to MW devices [6,7]. A breakthrough transition to the atomic resolution ($\sim 0.2-0.3$ nm) was published in [8] after implementation of the tunnel microscopy principle in the NFMM. The potential of NFMM application for diagnostics of semiconductor materials and structures for the benefit of solid-state micro- and nano-electronics is undoubtful today [9]. Relevant studies applied microscopes both of nanometer [6,10–14], and micrometer resolution [15–18]. The situation with the studies on NFMM one may learn from the review papers and monographs [3,9,19–21].

The problem of obtaining quantitative information on electrophysical characteristics of the studied objects by means of NFMM, including structured ones, cannot be recognized today as totally resolved. In order to get such information a theory is needed that relates measured characteristics with the parameters of the studied object. The problem refers to a complicated geometry (often is not known clearly enough) of the microscope probes. Simplification assumptions are used for developing analytical models [22–28] that decrease the accuracy of description. An additional complicating factor is that the parameters of the models depend on the characteristics of the studied

object, i.e. must be specified in a self-agreed manner by the data of calibration measurements [15–18,29,30]. Nevertheless, today, by means of conventional NFMM it is succeeded to describe accurately enough simple objects with one parameter to be determined, e.g., to measure specific electrical conductivity of a homogeneous in volume material, or sheet resistance of a film structure [11–18]. For more complex structures containing several unknown parameters, the object characteristics can be determined by inverse problem solving, which, as a rule, is mathematically incorrect and non-linear. To resolve the inverse problem successfully the key requirement is a high accuracy of the theoretical model. The studies [31,32] noted a beneficial circumstance: in case of the probe (antenna) of regular coaxial shape the analytical model proposed in [16] becomes accurate enough for solving at least three-parameter inverse problems. The characterization performed in the [31] for the diode structure with the resolution of $10-60\,\mu$m — is an example of solving of the problem in question. Note that performance of relevant measurements requires application of microscopes with special (non-conventional) designs.

A conventional MW microscope is a frequency-selective device, since it is has resonator. Appearance for the last 10−15 years of commercial probing stations that operate in the frequency range up to ~ 100 GHz (such as Cascade Microtech) allows to produce a MW-spectrometer that combines locality of NFMM with measurements in a wide frequency interval within the same device. The method of volt-impedance (Z−V) spectroscopy of semiconductors proposed in [33] and proven experimentally in [32] enables obtainment of a full set of electrophysical characteristics of semi-conductor wit micron lateral resolution by solving the three-parameter inverse problem: concentration, mobility, type of free charge carriers, specific conductivity. As a result it has become possible to carry into the MW-range such informative methods of study of semiconductors as volt-farad (C−V) diagnostics [34] and the admittance spectroscopy (AS) [35–37]. Both methods were applied earlier at low (not more than 10 MHz) frequencies, due to which they did no provide for micron resolution. However, the possibility of obtaining additional information on the conductivity of structures with the Schottky barrier by means of the Z−V-method was implemented incompletely according to the publication [32]. The problem was insufficient accuracy of measurements of real part of impedance of the structures within the low-frequency ($f < 500$ MHz) region of the spectrum. This work has proposed solution of that problem and performed relevant study of semiconductor.

1. Impedance measurement accuracy

The Z−V-method developed in [32,33] is based on the measurement by using the probing station Cascade Microtech (CM) of the frequency spectrum of impedance of the probe−sample system $Z(f, U)$ as a function of the DC voltage U applied to the probe. Electrophysical parameters of the sample are determined by solving of corresponding inverse problem. At that, the impedance Z measurement accuracy has a definitive value. First, let's consider conventional system of measurements implemented in [32], when the spectrum $Z(f)$ is determined by the spectrum of the complex coefficient of reflection $S11(f) = \Gamma(f)$ (in the system of S-parameters) with direct connection of CM-probe to one of the ports of vector network analyzer. Here

$$\Gamma(f) = \frac{Z_0 - Z(f)}{Z_0 + Z(f)}, \tag{1}$$

where Z_0 — wave impedance of the connecting cable. Let the complex coefficient of reflection Γ_0 to be measured with an error $\Gamma = \Gamma_0 + \delta_\Gamma(1+i)$, i.e. we assume the error δ_Γ of measurement of real and imaginary parts Γ_0 to be similar, whereas $\delta_\Gamma \ll |\Gamma_0|$. As a result, the components of impedance $Z = R - iX$ are determined with an error $\delta_{R,X}$. In the low-frequency part of the spectrum $Z(f)$ there is the ratio $X \gg R$, Z_0 [32] (see also fig. 5), i.e. $|\Gamma_0| \approx 1$. Then, based on the formula (1) it is easy to obtain

$$\frac{\delta_X}{X} = \frac{X}{2Z_0}\,\delta_\Gamma, \tag{2a}$$

$$\frac{\delta_R}{R} = \frac{X}{2Z_0}\left(\frac{X}{R}\right)\delta_\Gamma. \tag{2b}$$

We can see far higher error of determination of the resistance $\delta_R/R \gg \delta_X/X$. In the measurements [32] for the range $f = 10-100$ MHz we took $X = 10^3-10^4\,\Omega$, $R = 5-50\,\Omega$ (the values R in the publication [32] were not determined reliably, but obtained herein (see fig. 5, *b*)). Then, at $\delta_\Gamma \approx 10^{-3}$, $Z_0 = 50\,\Omega$ we obtain $\delta_X/X \approx 10^{-2}-10^{-1}$, $\delta_R/R \approx 2-20$, it is what causes the above problem of determination of the resistance R.

Let's now consider the measurement scheme proposed herein. The vector network analyzer is connected to the input of MW-resonator, as shown in fig. 1, *b*. CM-probe is attached to the end of one of the resonator shoulders. In this case the reflection coefficient spectrum is presented as [18]:

$$\Gamma(f) = \frac{\frac{1-\beta}{Q_0} - 2i\left(\frac{f}{f_0} - 1\right)}{\frac{1+\beta}{Q_0} + 2i\left(\frac{f}{f_0} - 1\right)}, \tag{3}$$

where f_0 — resonance frequency, Q_0 — unloaded Q-factor, β — is the connection parameter. For the resonator model as a segment of two-wire line shown in fig. 2, *a*, the parameters f_0, Q_0, β are obtained in [18], if one takes the length $l_{\text{CM}} = 0$ in order to simplify the analysis. There are the following for the half-wave mod: $f_0 = c/\left[2l\left(1 + Z_0/(\pi X)\right)\right]$, $Q_0 = Z_0/R_\Sigma$, $\beta = \rho^2/(Z_0 R_\Sigma)$, $\rho = \pi Z_0(l_1 - l_2)/(2l)$, $R_\Sigma = \pi Z_0\delta + Z_0^2 R/X^2$, where c — light speed, δ — parameter of own losses of the resonator introduced into sect. 3, $l = l_1 + l_2$ — full length of the resonator ($l_1 > l_2$). The lengths of shoulders of resonator l_1, l_2 and CM-probel_{CM} are shown in fig. 1, *b*. Then, when considering the error of measurement of the coefficient Γ

we obtain errors of measurement of the impedance components:

$$\frac{\delta_X}{X} = \frac{X}{2Z_0}\left[\frac{(1+\beta)^2}{\beta Q_0}\right]\delta_\Gamma, \tag{4a}$$

$$\frac{\delta_R}{R} = \frac{X}{2Z_0}\left(\frac{X}{R}\right)\left[\frac{(1+\beta)^2}{\beta Q_0}\right]\delta_\Gamma. \tag{4b}$$

By comparing the expressions (2) and (4), we can see that the use of resonator scheme of measurements decreases the error of determination of impedance $(\beta Q_0)/(1+\beta)^2$ times, which in our case ($0.5 < \beta < 2$, $Q_0 \approx 100$) provides the multiple of 10–20 benefit for the accuracy.

2. Measurement system and studied sample

The spectrometer (fig. 1, *a*) contained resonator, whose two shoulders made of segments of semi-rigid coaxial cable RG-402, were connected by means of triple coaxial adapter SMA-KKK (socket–socket–socket) to the port *1* of the vector network analyzer (VNA) Anritsu MS46122B, as shown in fig. 1, *b*. VNA calibration was performed by means of SmartCal-of the module MN25208A of each of the working ranges: 40–70; 70–100; 140–180; 230–280 MHz. VNA operation control and registration of reflection $\Gamma(f)$ was performed by means of personal computer in the software package ShockLine™. The load of one of the spectrometer shoulders was coaxial-coplanar probe (Z-probe coaxial) Z067-V3N-GSG-150 of the station CM. Two resonators R1, R2 were manufactured for the frequencies: (R1) $f_0 \approx 55$ and 160 MHz; (R2) $f_0 \approx 85$ and 160 MHz, corresponding to $\lambda/2$, $3\lambda/2$ mods of each. The lengths of shoulders $l_{1,2}$ of resonators were estimated in advance. The estimate methodology is described in the next section. The task of calculation (in addition to obtainment of the frequency f_0 in required ranges) for the connection parameter β was not to be beyond the range 0.5–2 both without contact of probe to the sample (Air mod), and with the contact. In the latter case it was supposed that impedance of the probe $Z(f_0)$ takes the values (obtained in the publication [32]; expected values) were selected for $R(f_0)$. Within the specified range β there is a good matching of the resonator, when $|\Gamma(f_0)|^2 < -10$ dB, which provides sufficient accuracy of determination of the impedance Z. In case of matching that is close to ideal, there are $\beta \approx 1$, $|\Gamma(f_0)| < -40$ dB. As a result of calculation and a bit shortening of the free shoulder l_1 during the adjustment measurements, it was obtained: (R1) $l_1 = 110.8$ cm, $l_2 = 87.7$ cm; (R2) $l_1 = 66.5$ cm, $l_2 = 50.4$ cm. In the sample measurements, the shoulder l_1 was elongated by the value Δ and 2Δ ($\Delta \approx 1$ cm) by using the inserts in the form of SMA- of the plug–socket connectors. It ensured three independent measurement Z per $\lambda/2$ mod of each resonator with insignificant frequency shift f_0 with matching that fell within the specified range of values β. The required matching of resonators for the parameter β on $3\lambda/2$ mod was also achieved by the insert 3Δ into the shoulder l_1. The examples of obtained resonance curves $|\Gamma(f)|$ in contactless and contact modes are given in fig. 3, *b* and 4.

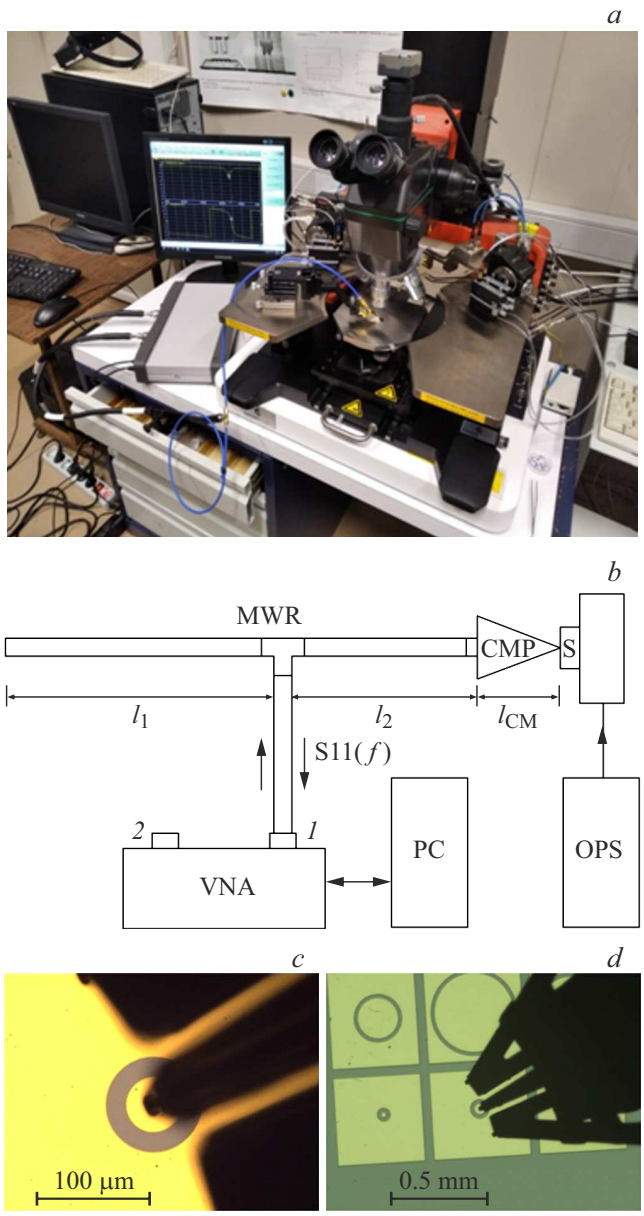

Figure 1. *a* — resonance CM-spectrometer; *b* — block diagram of the spectrometer. MWR — MW resonator, CMP — CM-probe, S — studied sample, VNA — vector network analyzer, PC — personal computer, OPS — optical-mechanical positioning system; *c* — CM-probe approached to the antenna S5; *d* — antenna module in contact of CM-probe with antenna S5.

Homogeneous monocrystalline plate GaAs with the thickness of 0.43 mm was studied, on whose surface a system of concentric Schottky contacts (antenna system) was formed in the form of modules covering the whole surface 1.5×1.5 mm, consisting of nine antenna of various diameters. The same sample was studied in the [32].

For the microwave measurements we used two antennas S4 and S5 (located in one of the modules in the middle of the sample) with the diameter a of central contact equal to 27 and 57 μm, accordingly. The contact of the CM-probe with each antenna (fig. 1, *c, d*) was done by means of the optical positioning system. The shift voltage between the contact pads of antennas $U = 0$. At that, near to the metal–semiconductor boundary, there is formation of depleted layer with the thickness of $d = 77.5$ nm with undisturbed concentration of electrons $n_0 \approx 2 \cdot 10^{17}\,\mathrm{cm}^{-3}$, contact difference of potentials $U_c = 0.75$ V [32]. The measured impedance $Z(f_0)$ is formed by interaction of the antenna with the structure that includes depleted layer of semiconductor and the underlaying region with undisturbed concentration. As shown in [31], the concentric antenna of the geometry in question is a monopole, i. e. its impedance is determined only by the diameter a of the central contact and is independent on the size of external metallized pad. The scale a determines also resolution power of the method in question. The sample probing was performed at lower (10^{-2} mW) power of signal VNA, excluding non-linear distortions of impedance Z.

3. Measurement procedure

The task was to determine the impedance $Z(f_0)$ by the measured resonance characteristics $\Gamma(f)$ of the probe–sample system. For this purpose we performed calculations by using the equivalent scheme of the MW-circuit of the spectrometer shown in fig. 2, *a*.

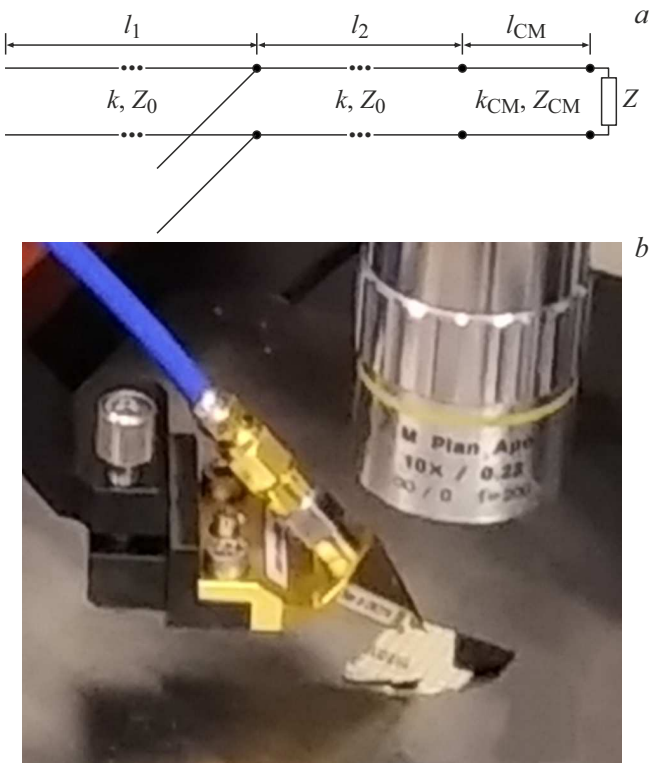

Figure 2. *a* — equivalent diagram of resonator with the CM-probe and load; *b* — CM-probe in the Air mode.

In this scheme the resonator and CM-probe (fig. 2, *b*) are given as the segments of two-wire lines with the wave impedances Z_0, Z_{CM} and wave vectors k, k_{CM}, whereas $Z_0 = Z_{CM} = 50\,\Omega$, $k = k_0\sqrt{\varepsilon_L}(1 + i\delta_L)$, $k_{CM} = k_0\sqrt{\varepsilon_{CM}}(1 + i\delta_{CM})$, $k_0 = 2\pi f/c$, ε_L, δ_L — are permittivity and own losses of the coaxial cable, ε_{CM}, δ_{CM} — similar parameters of the two-wire line simulating the probe. The studied sample was considered as the load Z at the end of the CM-line. The calculation of the resonance characteristics was performed by using the formulas

$$\Gamma(f) = \frac{Z_0 - Z(f)}{Z_0 + Z(f)}, \tag{5}$$

$$Z(f) = \frac{Z_1(f)Z_2(f)}{Z_1(f) + Z_2(f)}, \tag{6}$$

$$Z_1(f) = -iZ_0\,\mathrm{ctg}\big(k(f)l_1\big), \tag{7a}$$

$$Z_2(f) = \frac{Z_0[Z^{in}_{CM}(f) + iZ_0\,\mathrm{tg}\big(k(f)l_2\big)]}{iZ^{in}_{CM}(f)\,\mathrm{tg}\big(k(f)l_2\big) + Z_0}, \tag{7b}$$

$$Z^{in}_{CM}(f) = \frac{Z_0[Z + iZ_0\,\mathrm{tg}\big(k_{CM}(f)l_{CM}\big)]}{iZ\,\mathrm{tg}\big(k_{CM}(f)l_{CM}\big) + Z_0}, \tag{7c}$$

where l_1, l_2 — the lengths of segments of lines forming the resonator, and l_{CM} — the length of the line simulating the CM-probe (fig. 2, *a*, as well as fig. 1, *b*). Note, that in formulas (7) the frequency dependence of impedances is determined by the phasing constant on each segment of the line, i. e. the value $\sqrt{\varepsilon}l$, but not the parameters ε, l individually. This is why for the coaxial cable we assumed $\varepsilon_L = 2$ (fluoroplast), and the length of shoulders $l_{1,2}$ were determined by measurements. For the CM-probe, vice versa, we used the geometrical length $l_{CM} = 4.5$ cm, and permittivity ε_{CM} was found in the experiment.

The impedance of the sample Z can be found only in the case when the parameters of the equivalent scheme in fig. 2, *a* are known, therefore, we performed measurement with disconnected CM-probe. The parameters of coaxial lines forming the resonator were found based on the condition of the best correlation between the measured and estimated resonance curves by minimization of discrepancy:

$$N(l_1, l_2, \delta_L) = \int_{f_a}^{f_b} [|\Gamma_e(f)| - |\Gamma_t(f, l_1, l_2, \delta_L)|]^2 df, \tag{8}$$

where $\Gamma_{e,t}$ — experimental and theoretical resonance curves. Calculation of the function $\Gamma_t(f, \varepsilon_{CM}, \delta_{CM})$ by using the formulas (5)–(7) is performed at $l_{CM} = 0$ (probe disconnected), $Z = \infty$ (open line). In this case the formula (7b) is similar to (7a) with replacement of $l_1 \to l_2$. For finding the minimum of discrepancy (8) the software package Mathcad was used:

$$\mathbf{Y} = \begin{pmatrix} Y_1 \\ Y_2 \\ Y_3 \end{pmatrix} = Minimize(N, l_1, l_2, \delta_L). \tag{9}$$

The integrating range of frequencies $f_a - f_b$ in (8) was determined as $|f_{a,b}/f_0 - 1| = 1/Q_0$, where the resonance frequency and Q-factor of the resonator f_0, Q_0 were found by minimization of discrepancy (8) $N(f_0, Q_0, \beta)$, in which the function (3) was used as $\Gamma_t(f, f_0, Q_0, \beta)$. Note that calculated lengths $l_{1,2}$ appeared to be close to their geometrical values. For the resonator without insert ($\Delta = 0$) the lengths $l_{1,2}$ are given above.

By measuring the resonance characteristics $\Gamma_e(f)$ with the connected CM-probe without contact with the sample (Air mode) we determined parameters ε_{CM}, δ_{CM} by the minimum of discrepancy (8), as the functions $N(\varepsilon_{CM}, \delta_{CM})$. At that, the function $\Gamma_t(f)$ was calculated by the formulas (5)–(7), where $Z = \infty$, and the values determined at the first stage were used as the parameters $l_{1,2}$, δ_L. Examples of the obtained values of the parameters of spectrometer are given in Table at $\Delta = 0$. As expected, CM-probe has considerably higher own losses δ_{CM} versus the losses δ_L in coaxial cable. Nevertheless, connection of the probe decreases a bit (within 10%) the Q-factor of the resonator Q_0, because $l_{CM} \ll l_{1,2}$.

Note an important circumstance, which must be taken into account when searching for the parameters of the model of spectrometer and impedance Z in (5)–(7) by minimization of discrepancy (8). The function $|\Gamma_t(f)|$ has the same form with two different sets of parameters of the formulas (5)–(7). It is easy to understand, if write the spectrum $|\Gamma_t(f)|$ by using the representation (3). We obtain similar functions $|\Gamma_t(f)|$ when replacing $\beta \to 1/\beta$, $Q_0 \to \beta Q_0$. Unambiguous resolution (9) can be obtained, by comparing the phases $\varphi_{e,t}(f)$ of functions $\Gamma_{e,t}(f)$. Different set of the found model parameters (5)–(7) corresponds to different sings of the derivative $d\varphi_t(f)/df|_{f=f_0}$ near to the resonance frequency f_0, which can be clearly seen from the formula (3). Therefore, if the functions obtained in the software (9) and measured one $\varphi_{e,t}(f)$ have different signs of derivative (i. e. incorrect solution is found), then one must change in the software (9) the range for the solution finding, after which we will obtain a correct set of the parameters.

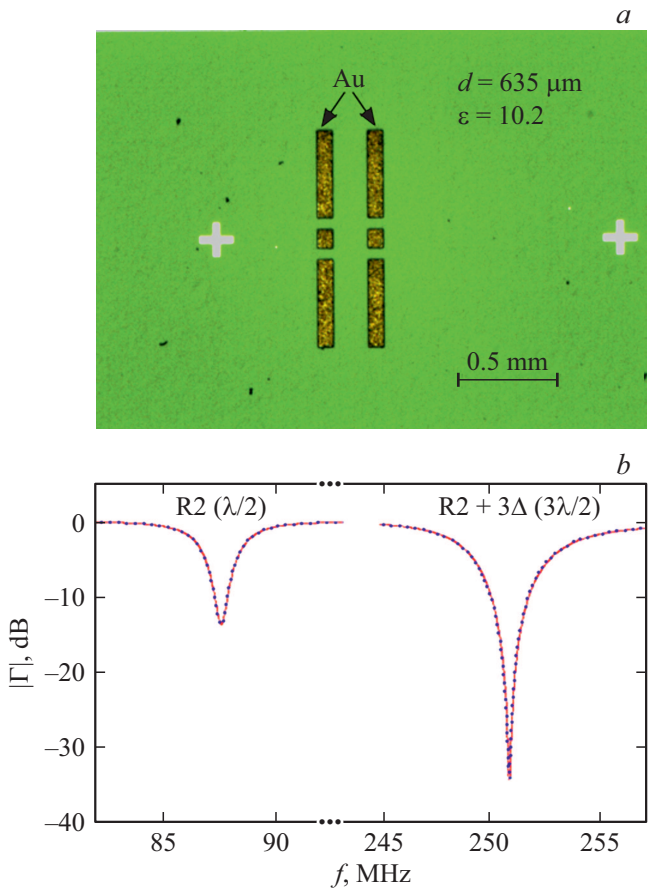

Figure 3. *a* — reference load with impedance $Z = \infty$; *d*, ε — thickness and permittivity of the substrate; *b* — calibration spectra. The mods $\lambda/2$ and $3\lambda/2$ of resonator R2 with the insert $\Delta = 0$ and 3Δ. Solid lines — measurements in the Air mode, dashed lines — reference load measurements.

Parameters of the spectrometer

f_0, MHz	55	85	160	250
$\delta_L \cdot 10^3$	6.0	5.4	5.1	4.4
ε_{CM}	1.05	1.06	1.19	1.11
$\delta_{CM} \cdot 10^3$	8.6	7.3	9.6	10.2

4. Research results

4.1. Measurement of impedance

The process of measurement of the impedance Z was accompanied by calibration, because the obtained parameters of the spectrometer are slightly varying in different measurement cycles depending on the quality of the connections assembling, temperature and humidity in the laboratory. For the purpose of accurate determination of Z we performed calibration measurements in the beginning and the end of each measurement cycle. Calibration can be performed by using the reference load $Z = \infty$ of the set of standards Z of the CM station (fig. 3, *a*). However, the measurements of functions $\Gamma(f)$ in case of contact of the probe to the reference load and in the Air mode have shown identical spectra, as can be seen in fig. 3, *b*. This is why a more simple measuring process was applied with calibration in the Air mode. Calibration was performed only with the connected CM-probe. At that the parameters of probe ε_{CM}, δ_{CM} were considered as fixed (see table), and characteristics of coaxial cables were clarified l_1, l_2, δ_L. The measurements in fig. 3, *b* demonstrate also that in contact of CM-probe with metallic surfaces of the reference load no parasitic impedance occur. The same conclusion can be extended to metallic surfaces of antennas, i. e. the found impedance of the sample Z describes the Schottky contact metal–semiconductor.

Determination of the impedance $Z = R - iX$ was performed by measurement of the spectrum $\Gamma_e(f)$ in the

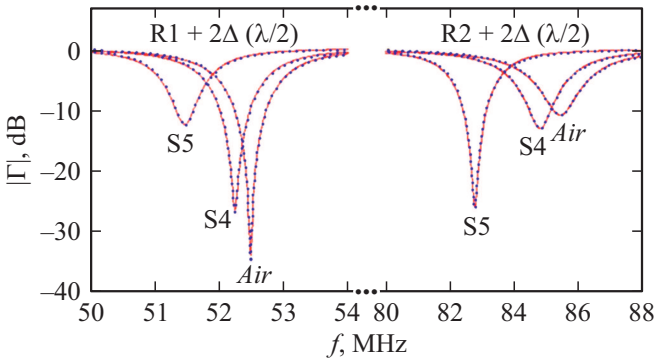

Figure 4. Resonance spectra in the calibration mode (Air) and on the antennas S4, S5. The $\lambda/2$ mod of resonators R1 (on the left), R2 (on the right) with the insert 2Δ. Solid lines — measurements, dashed lines — calculation.

contact of CM-probe with antennas S4, S5 on the surface of semiconductor plate (fig. 1, *c*, *d*). The components of impedance R, X were calculated by minimization of discrepancy (8), as the function $N(R, X)$. When calculating the spectra $\Gamma_t(f, R, X)$ in the model (5)–(7) the values of spectrometer parameters obtained during calibration were used. In (7c) we taken the sample impedance as independent on the frequency $Z = Z(f_0)$, since resonators R1, R2 had quite high Q-factor ($Q_0 \approx 100$), and all calculations were performed within the narrow range near to resonance frequency $|f/f_0 - 1| \le 1/Q_0$. Examples of the obtained spectra are given in fig. 4. We can see very good accordance of the calculations and measurements after putting the found parameters of spectrometer and sample impedance into theoretical model (5)–(7). It is seen also quite high informativeness of the spectrum $\Gamma(f)$ for the Schottky contact characteristics for both antennas.

The results of measurement of the reactance X and resistance R are given in fig. 5. The dependencies $X(f)$, $R(f)$ obtained by the methods of non-resonance (NS) [32] and resonance (RS) spectroscopies are given. A small difference between the resonance frequencies for $\lambda/2$-mod of each resonator corresponding to three values Δ, is not shown in fig. 5 at all. In Fig. 5, *a* we can see very good accordance of the spectra $X(f)$ measured by both methods, which indicates reliability of the obtained data. Note also insignificant spread in values $X(f)$ from the point to point (over 10^3 of discrete frequencies in NS-measurements) in the range $f > 20-30$ MHz, which was forecasted in the analysis made in section 1. Other situation is observed for the spectra $R(f)$ (fig. 5, *b*). Low-frequency part NS-of spectra ($f < 200-300$ MHz) is too noisy. Moreover, in the region of low frequencies the value R at individual frequencies takes negative values, because, due to the noises of the NS-spectrometer, the measured coefficient of reflection $|\Gamma| = |\Gamma_0| + \delta_\Gamma$ may have the values $|\Gamma| > 1$, because $|\Gamma_0| \approx 1$ at $X \gg Z_0 = 50\,\Omega$. As a result NS-the spectra $R(f)$ at low frequencies in linear scale seem to be symmetrical relative to the level $R = 0$. Fig. 5, *b* shows spectra $R(f)$ in logarithmical scale, where no values $R < 0$ are viewed.

Therefore, NS do not allow to reliably conclude on the resistance of the probe R in the low-frequency part of the spectrum, whereas the spread in values is increased abruptly with the decrease of the antenna diameter. Otherwise, RS provides far more stable values R. In Fig. 5, *b* it can be seen clearly the excess of R (up to two orders) over the high-frequency value $r_0 = 1-2\,\Omega$. The RS-measurements demonstrate monotonous growth of the resistance with the decrease of frequency, due to which R reach $10-100\,\Omega$ at low frequencies of the spectrometer. With the decrease of the diameter a of contact, there is a more abrupt growth of R. Note that the unreliable data obtained in [32] on the excessive resistance R did not impede solution of the problem of that study — determination of main electrophysical characteristics of semiconductor. The low-frequency part of spectrum $R(f)$ bears an important additional information on the conducting properties of the Schottky contact.

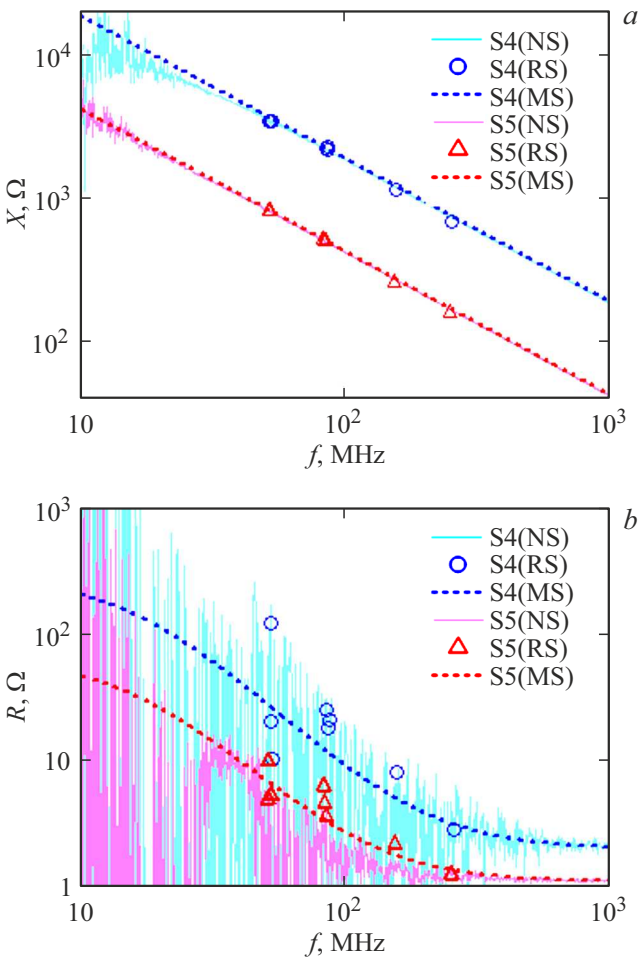

Figure 5. Reactance (*a*) and resistance (*b*) of the sample obtained on the antennas S4, S5. NS — non-resonance spectroscopy (solid lines), RS — resonance spectroscopy (symbols), MS — model spectra (dashed lines).

4.2. Deep states

The found excessive resistance $R > r_0$ in the range 10−250 MHz is not explained by elementary theory of the Schottky contact [38,39]. According to that theory, the impedance of the contact Z is described by the equivalent scheme shown in fig. 6, *a*, where

$$R_c = \frac{r_c}{S_a}, \quad C_d = \frac{\varepsilon_0 \varepsilon' S_a}{d}, \quad r_0 \approx \frac{1}{2\sigma_0 a}. \qquad (10)$$

Here $d(U = 0) = 77.5$ nm — is the thickness of depleted layer at zero bias voltage [32], $S_a = \pi a^2/4$ — area of the contact, ε_0 — electrical constant of vacuum, $\varepsilon' = 12.9$ — permittivity of GaAs, σ_0 — conductivity of undisturbed region of semiconductor. We determined the resistance $r_c = 5 \cdot 10^4\ \Omega \cdot \text{cm}^2$ by measurement at d.c.. In the range $f > 1$ MHz there are $R_c \gg 1/(\omega C_d)$ $(\omega = 2\pi f)$, as a result of which the equivalent serial resistance $1/\left(R_c(\omega C_d)^2\right) \ll r_0 = 1{-}2\,\Omega$ at $f > 10$ MHz, $\sigma_0 \approx 84\ (\Omega \cdot \text{cm})^{-1}$ [32]. This is why in the frequency range in question we may ignore the impact of R_c to the contact impedance. By performing calculations under the equivalent scheme given in Fig. 6, *a*, for the antennas S4, S5 we obtain MS dependences $X(f)$, shown in fig. 5, *a* as dashed lines. At the same time, the calculation gives constant resistance $R(f > 10\,\text{MHz}) \approx r_0$, which is the resistance of alternating current spreading in undisturbed region of semiconductor under the depleted layer. To the contrary, the performed measurements gave $R \gg r_0$ in the low-frequency part of the spectrum.

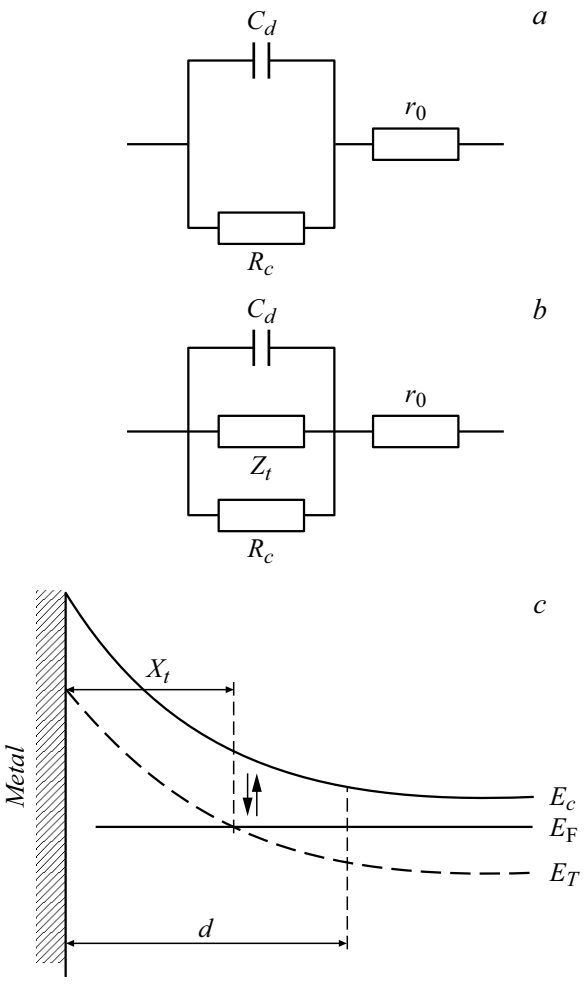

Figure 6. *a* — equivalent scheme of the Schottky contact; *b* — equivalent scheme subject to deep states; *c* — levels of energy of the Schottky contact with deep states. E_F — Fermi level, E_c — dopant level, E_T — deep level.

Excessive resistance in the spectrum $R(f)$ can be explained by the presence of deep states (traps) in semiconductor, related with impurities or defects [40]. In the Schottky barrier, the Fermi level E_F crosses the deep level E_T at a distance x_t from the metal−semiconductor boundary, as shown in fig. 6, *c*. In approximation of total depletion it is easy to obtain

$$\frac{x_t}{d} = 1 - \sqrt{\frac{E_F - E_T}{U_c}}. \qquad (11)$$

The a.c. voltage results in oscillations of the Fermi level position, due to which the deep levels are overcharged. Main contribution into overcharge is made by the traps made of thin (~ 10 nm) layer of semiconductor located near to x_t. As a consequence of overcharge of traps, the equivalent scheme of the contact is transformed due to additional complex impedance Z_t [37] (fig. 6, *b*), determined by serial connection of corresponding capacitance and resistance. According to [37], there are

$$Z_t = \frac{1}{\Delta C S_a}\left(\frac{-i}{\omega} + \tau\right), \qquad (12)$$

$$\Delta C = \frac{\varepsilon_0 \varepsilon'}{d}\,\frac{n_t}{n_0}\,\frac{1 - \frac{x_t}{d}}{1 + \frac{x_t}{d}\,\frac{n_t}{n_0}}. \qquad (13)$$

Here, τ — is the time of the traps filling relaxation, n_t — is the traps concentration. The results of calculation of the impedance spectrum $Z(f)$ by the equivalent scheme in fig. 6, *b* are shown in fig. 5 as model spectra MS. The calculations have taken the following values of the trap parameters: $\tau = 10^{-8}$ s, $n_t/n_0 = 5 \cdot 10^{-2}$, $x_t/d = 0.5$ at the depth of their level $E_F - E_T = 0.2$ eV. As we can see, model spectra $R(f)$ in fig. 5, *b* are in a good agreement with the experimental data. Subject to (12), (13) in the diagram of fig. 6, *b* we will obtain $C_d \leq \text{Im}[Z^{-1}(\omega)]/\omega \leq C_d + \Delta C S_a$. In the case in question we have the ratio $\Delta C S_a \ll C_d$. As a result, the capacitance component of the impedance Z_t virtually has no impact to the spectrum $X(f)$,due to which the MS curves in fig. 5, *a* calculated by the equivalent schemes in fig. 6, *a, b*, coincide.

Parameters of deep states are usually studied by the AS method within the range of frequencies $f < 10$ MHz with the contact size $a > 100\,\mu$m [37,41–44]. For this special purpose the contact with Schottky barrier is created. The study of traps with the characteristics obtain herein by means of conventional AS at room temperature is complicated, because in case of macroscopic contact their

resistance is overlapped by the resistances of depleted layer R_c and spreading r_0. In fact, by using the equivalent scheme in fig. 6, *b*, the contact impedance can be represented as

$$Z = -\frac{i}{\omega C_d} + \frac{R_t f(\omega)}{1 + \omega^2 \tau_d^2 f^2(\omega)} + r_0, \qquad (14)$$

where $R_t = \tau/(\Delta C S_a)$, $f(\omega) = (1 + \omega^2\tau^2)/\omega^2\tau^2$. Formula (14) gives asymptotic of the resistance spectrum: low-frequency ($\omega\tau \ll 1$) $R = R_S = R_t(\tau/\tau_d)^2 + r_0$ and high-frequency ($\omega\tau \gg 1$) $R = R_t/(\omega\tau_d)^2 + r_0$, where $\tau_d = R_t C_d$. For the values of parameters taken in the calculations we have the resistance per the square unit of the contact $r_t = R_t S_a = 2.8\,\Omega \cdot \text{cm}^2$ at $\tau_d = 4.2 \cdot 10^{-7}$ s. Then, for the contacts S4 and S5 we will obtain low-frequency resistance of saturation $R_S = 281$ and $63\,\Omega$ accordingly, i. e. $R_S \gg r_0 \approx 2$ and $1\,\Omega$. Saturation of the function $R(f)$ is achieved at $f \approx 3{-}5$ MHz, therefore, in fig. 5, *b* there is only a trend to saturation. With the decrease of frequency in the range $f < 1$ MHz, the function starts rising monotonously $R(f)$ under impact of the resistance R_c, which we ignored in the formula (14). In the range $f > 50$ MHz there is a high-frequency (descending $\propto f^{-2}$) dependence of the excessive resistance, so that at $f > 250$ MHz we obtain $R \approx r_0$. Therefore, the obtained effect is that in the range of frequencies $10\,\text{MHz} < f < 200\,\text{MHz}$ it is $r_0 < R < R_S$ at $R_S \gg r_0$. The mentioned effect is clearly observed only with a small enough diameter of the contact $a < 100\,\mu$m, since $R_S \sim a^{-2}$, whereas $r_0 \sim a^{-1}$, i. e. ratio $R_S/r_0 \sim a^{-1}$. The function $Re\left(Z(\omega)^{-1}\right)/\omega$ has the maximum, which, as easily derived from the formula (14), is implemented at $\omega\tau = 1$ and related with the presence of excessive resistance of the contact. Measurement of that maximum that disappears with the increase of the diameter a, provides the easiest method for determination of the time for overcharging the traps τ [37]. In the model in question of the studied sample the maximum is implemented at the frequency of $f = 16$ MHz. Subject to the mentioned challenges in the study of traps at low-frequency measurements of the admittance of macroscopic contacts, a passage by temperature is performed in the conventional AS, starting from the temperature of liquid helium In case of low temperatures the time of the traps overcharge τ is increased, which makes possible to measure the change of contact capacitance related with the traps at low frequencies. Therefore, the NS- RS-method developed by us, which is in fact the MW-analog to conventional AS, provides for not only locality of measurements, but also permits to determine the parameters of the traps at room temperature.

Introduce efficient conductivity of the depleted layer $\sigma_t = d/r_t$. In the case in question we obtain $\sigma_t = 2.8 \cdot 10^{-6}(\Omega \cdot \text{cm})^{-1}$. It is the conductivity σ_t that was determined in the [32] from solution of the three-parameter inverse problem by using the low-frequency spectrum $R(f)$ measured unreliably. Nevertheless, for the antennas S4, S5 in [32] we have obtained $\sigma_t = (1.4, 3.2) \cdot 10^{-6}\ (\Omega \cdot \text{cm})^{-1}$ at $U = 0$ — the values that are in good agreement with the results hereof. Note that in the trap model in question, according to (12), there is a complex conductivity of depleted layer $\tilde{\sigma}_t = i\sigma_t\omega\tau/(1 + i\omega\tau)$, from -due to which the inverse problem becomes four-parameter with the parameter τ to be determined additionally.

Note also, that the excessive resistance found herein $R(f) > r_0$ determines the Joule losses in the barrier contact within some frequency interval (10−250 MHz as in our case). Such observation could be interesting for a series of device applications of the Schottky high-frequency diodes of micron and submicron diameters, in particular, for mixers. E.g., for $a = 0.5\,\mu$m, by using equivalent scheme in fig. 6, *b*, in the range $f \approx 1$ GHz it is not hard to obtain $R \approx 600\,\Omega > r_0 \approx 100\,\Omega$, i. e. the losses at the difference frequency of mixer based on the studied material are generally caused by the excessive resistance.

Conclusion

The study has evolved the method of the microwave resonance spectroscopy of semiconductors that exceeds potential capabilities of the non-resonance Z−V-spectroscopy developed in [32,33]. The problem Z−V-spectroscopy referring to the determination of local values of main electrophysical characteristics of semiconductor is successfully resolved by means of the NS-measurements within the microwave range. Obtainment of additional information on the resistive properties of the Schottky contact required change of the measurement technique. It is the purpose the RS-method is used for. The method allowed to study the spectrum of resistance of the semiconductor structure with the Schottky barrier with the lateral resolution of 30−60 μm. The excessive resistance of the Schottky contact observed within the range of 50−250 MHz is highly likely related with the presence of deep states in the studied material. In order to confirm the proposed hypothesis it is expedient to perform additional studies. The capabilities of the developed RS- and NS-techniques based on the CM probing station allow to perform the measurements for the lower diameter contacts, up to $a \sim 3{-}5\,\mu$m, within the frequency range up to 20−30 GHz and higher. It is expedient to increase the number of the working frequencies RS in the informative part of the spectrum $R(f)$. It is also interesting to perform parallel measurements by using independent methods, e.g., the method of deep-level transient spectroscopy (DLTS).

Combination of NS- and RS-measurements provides experimental material in the form of spectra $R(f)$, $X(f)$, necessary for inverse problems solution to semiconductors characterization. The studies [31,32] demonstrated the possibility of resolution of the three-parameter inverse problems solving. Application of coaxial antennas provides for necessary accuracy of the analytical model used for solving of them. Further development Z−V-of spectroscopy is seemed as application thereof to planar semiconductor structures.

Note that even for material, which is homogeneous by depth, the application of the Z−V-method is related with the study of the structure in the form of depleted layer above the undisturbed region of semiconductor. Thanks to creation of such a structure, it is succeeded to separately determine the concentration and mobility of the charge carriers. The third parameter to be determined is conductivity of the depleted level. For more complicated structures (e.g., film−substrate system) Z−V-technique will require solving of the inverse problem with a number of determined parameters that exceed three. Because of mathematical incorrectness of the problem the capabilities of such diagnostics need for a separate study.

In this embodiment Z−V-spectroscopy is a non-destructive, but contact method. The system of antennas formed on the sample surface can be removed by simple process operations after completion of measurements. Similar contactless measurements require development of special micro antennas. It is fundamental to preserve regular geometrical shape of the contactless antenna, in particular, concentric shape applied by us. The specified requirement is caused by the need for the solving of inverse problem, as a component of the developed method. C−V-diagnostics of semiconductors by using conventional NFMM of nanometer resolution was done in the studies [6,11,12,14]. The measurement performed therein did no allow to obtain a set of electrophysical parameters of the studied samples in the scope achieved in the [31,32]. One (but there are more) of causes for the arising challenges seems to be a complex geometry of existing nanometer probes, not allowing to perform accurate enough simulation. The applied technique of CM-measurements, very likely, will allow to make the resolution power of the spectrometer up to $3-5\,\mu$m. The issue of the possibility to have a progress into nanometer resolution still remains open. For separate determination of the concentration and mobility of carriers it is fundamentally important to develop the technique of measurement not only for imaginary (capacitance C), but also for real (resistance R) part of the impedance Z. The latter is important also for the study of conductive properties of the depleted layer performed herein.

One more time we note the significance of analytical models describing electrodynamics of the probe−sample system. In a series of publications the studies of potential capabilities of NFMM (resolution power, sensitivity, etc.) are performed based on computer simulation by using the finite element methods [45–50]. Hand made or commercial software programs are used for the electromagnetic simulation. Sometimes, based on the corresponding calculations quantitative characterization is performed for the samples of a quite simple structure [3,48–50]. Conceptual disadvantage of that approach is a long time for solving of direct problem. Thus, in the publication [47] for NFMM of a certain configuration and the sample with the specified permittivity the time for calculation of resonance characteristic was several hours. When proceeding with the inverse problems (in particular, for complex structures) the time of calculations is a key parameter. Algorithms of such problems solving use iterative descent with step-by-step solving of direct problem. Based on our experience, several hundreds of iterations are required even for simple objects (often thousands). As a result, the determination of characteristics of the studied object becomes virtually impossible in real time. The efforts taken to reduce the time costs [51] have not yet resulted in significant improvement of the situation. Moreover, modelling of the NFMM probe shape is a separate problem even with the presence of its microimages in several projections. As a rule, determination of geometrical parameters of the model requires additional calibration measurements, which increases the time for calculations additionally. In our opinion, today, only analytical models of the probes allow to develop efficient algorithms of inverse problems solving for near field microscopy.

Funding

The used equipment was provided by the Center of Shared Use of the Institute for Physics of Microstructures RAS (IPM RAS) “. Physics and technology of micro- and nano- structures“.

Conflict of interest

The authors declare that they have no conflict of interest.

References

[1] J.F. Power. Rev. Sci. Instrum., **73**, 4057 (2002). DOI: 10.1063/1.1517054
[2] J. Krupka. Meas. Sci. Technol., **24**, 062001 (2013). DOI: 10.1088/0957-0233/24/6/062001
[3] K. Lai, W. Kundhikanjana, M.A. Kelly, Z.-X. Shen. Appl. Nanosci., **1**, 13 (2011). DOI: 10.1007/s13204-011-0002-7
[4] C. Gao, T. Wei, F. Duewer, Y. Lu, X.-D. Xiang. Appl. Phys. Lett., **71**, 1872 (1997).
[5] V.V. Talanov, A. Scherz, R.L. Moreland, A.R. Schwartz. Appl. Phys. Lett., **88**, 134106 (2006). DOI: 10.1063/1.2189147
[6] H.P. Huber, I. Humer, M. Hochleitner, M. Fenner, M. Moertelmaier, C. Rankl, A. Imtiaz, T.M. Wallis, H. Tanbakuchi, P. Hinterdorfer, P. Kabos, J. Smoliner, J.J. Kopanski, F. Keinberger. J. Appl. Phys., **111**, 014301 (2012). DOI: 10.1063/1.3672445
[7] A. Tselev, N.V. Lavrik, I. Vlassiouk, D.P. Briggs, M. Rutgers, R. Proksh, S.V. Kalinin. Nanotechnology, **23**, 385706 (2012). DOI: 10.1088/0957-4484/23/38/385706
[8] J. Lee, C.J. Long, H. Yang, X.-D. Xiang, I. Takeuchi. Appl. Phys. Lett., **97**, 18311 (2010). DOI: 10.1063/1.3514243
[9] S. Berweger, T.M. Wallis, P. Kabos. IEEE Micrwave Mag., **21**, 36 (2020). DOI: 10.1109/MMM.2020.3008305
[10] G. Gramse, M. Kasper, L. Fumagalli, G. Gomila, P. Hinterdorfer, F. Kienberger. Nanotechnology, **25**, 145703 (2014). DOI: 10.1088/0957-4484/14/38/145703
[11] O. Amster, F. Stanke, S. Friedman, Y. Yang, St.J. Dixon-Warren, B. Drevniok. Microelectron. Reliability, **76−77**, 214 (2017). DOI: 10.1016/j.microrel.2017.07.082

[12] S. Hommel, N. Killat, A. Altes, T. Schweinboeck, F. Kreupl. Microelectron. Reliability, **76–77**, 221 (2017). DOI: 10.1016/j.microrel.2017.06.050
[13] S. Berweger, G.A. MacDonald, M. Yang, K.J. Coakley, J.J. Berry, K. Zhu, F.W. DelRio, T.M. Wallis, P. Kabos. NanoLett., **17**, 1796 (2017). DOI: 10.1021/acs.nanolett.6b05119
[14] A. Buchter, J. Hoffman, A. Delvallee, E. Brinciotti, D. Hapiuk, C. Licitra, K. Louarn, A. Arnoult, G. Almuneau, F. Piquemal, M. Zeier, F. Kienberger. Rev. Sci. Instrum., **89**, 023704 (2018). DOI: 10.1063/1.5015966.
[15] A.N. Reznik, E.V. Demidov. J. Appl. Phys., **113**, 094501 (2013). DOI: 10.1063/1.4794003
[16] A.N. Reznik, S.A. Korolyov. J. Appl. Phys., **119**, 094504 (2016). DOI: 10.1063/1.4943068
[17] A.N. Reznik, S.A. Korolyov, M.N. Drozdov. J. Appl. Phys., **121**, 164503 (2017). DOI: 10.1063/1.4982676
[18] S.A. Korolyov, A.N. Reznik. Rev. Sci. Instrum., **89**, 023706 (2018). DOI: 10.1063/1.5013113
[19] B.T. Rosner, D.W. Van der Weide. Rev. Sci. Instrum., **73**, 2505 (2003). DOI: 10.1063/1.1482150
[20] S.M. Anlage, V.V. Talanov, A.R. Schwartz. *„Principles of Near-Field Microwave microscopy", in Scanning Probe Microscopy: Electrical and Electromechanical Phenomena at the Nanoscale*, ed. by S. Kalinin, A. Gruverman (Springer Verlag, Berlin, 2007), p. 215–253.
[21] A. Imtiaz, T.M. Wallis, P. Kabos. IEEE Micrwave Mag., **15**, 52 (2014). DOI: 10.1109/MMM.2013.2288711
[22] D.E. Steinhauer, C.P. Vlahacos, S.K. Dutta, F.C. Wellstood, S.M. Anlage. Appl. Phys. Lett., **71**, 1736 (1997).
[23] C. Gao, X.-D. Xiang. Rev. Sci. Instrum., **69**, 3846 (1998).
[24] C. Gao, B. Hu, P. Zhang, M. Huang, W. Liu, I. Takeuchi. Appl. Phys. Lett., **84**, 4647 (2004). DOI: 10.1063/1.1759389
[25] A.N. Reznik, N.V. Yurasova. J. Appl. Phys., **98**, 114701 (2005). DOI: 10.1063/1.2138798
[26] Z. Wang, M.A. Kelly, Z.-X. Shen, L. Shao, W.-K. Chu, H. Edwards. Appl. Phys. Lett., **86**, 153118 (2005). DOI: 10.1063/1.1891296
[27] A. Imtiaz, S.M. Anlage. J. Appl. Phys., **100**, 044304 (2006). DOI: 10.1063/1.2234801
[28] T. Nozokido, M. Ishido, R. Seto, J. Bae. J. Appl. Phys., **118**, 114905 (2015). DOI: 10.1063/1.4931149
[29] A. Imtiaz, T. Baldwin, H.T. Nembach, T.M. Wallis, P. Kabos. Appl. Phys. Lett., **90**, 243105 (2007). DOI: 10.1063/1.2748307
[30] A.N. Reznik, V.V. Talanov. Rev. Sci. Instrum., **79**, 113708 (2008). DOI: 10.1063/1.3020705
[31] A.N. Reznik, N.V. Vostokov, N.K. Vdovicheva, S.A. Korolyov, V.I. Shashkin. J. Appl. Phys., **122**, 244505 (2017). DOI: 10.1063/1.4995330
[32] A.N. Reznik, N.V. Vostokov, N.K. Vdovicheva, V.I. Shashkin. Tech. Phys., **64** (11), 1859 (2020). DOI: 10.1134/S1063784220110237
[33] A.N. Reznik, N.K. Vdovicheva. Tech. Phys., **64** (11), 1722 (2019). DOI: 10.1134/S1063784219110240
[34] D.K. Schroder. *Semiconductor Material and Device Characterization* (J. Wiley Sons, Inc., 2006)
[35] D.L. Losee. Appl. Phys. Lett., **21**, 54 (1972).
[36] D.L. Losee. J. Appl. Phys., **46**, 2204 (1975).
[37] J.L. Pautrat, B. Katircioglu, N. Magnea, D. Bensahel, J.C. Pfister, L. Revoil. Solid-St. Electron., **23**, 1159 (1980).
[38] A.M. Cowley, H.O. Sorensen. IEEE Trans. Microwave Theory Techn., **MTT-14**, 588 (1966).
[39] S.M. Sze, K.K. Ng. *Physics of Semiconductor Devices* (J. Wiley Sons, Inc., 2007)
[40] G.M. Martin, A. Mitonneau, A. Mircea. Electron. Lett., **13**, 191 (1977).
[41] G. Vincent, D. Bois, P. Pinard. J. Appl. Phys., **46**, 5173 (1975).
[42] C. Ghezzi. Appl. Phys. A., **26**, 191 (1981).
[43] S.R. Forrest, O.K. Kim. J. Appl. Phys., **53**, 5738 (1982).
[44] A.V. Murel, V.B. Shmagin, V.L. Krukov, S.S. Strelchenko, E.A. Surovegina, V.I. Shashkin. Semicond., **51** (11), 1485 (2017). DOI: 10.1134/S1063782617110197
[45] M. Golosovsky, E. Maniv, D. Davidov, A. Frenkel. IEEE Trans. Instr. Meas., **51**, 1090 (2002). DOI: 10.1109/TIM.2002.806006
[46] A. Karbassi, D. Ruf, A.D. Bettermann, C.A. Paulson, D.W. Van der Weide, H. Tanbakuchi, R. Stancliff. Rev. Sci. Instrum., **79**, 094706 (2008). DOI: 10.1063/1.2953095
[47] C. Balusek, B. Friedman, B. Oetiker, A. Babajanyan, K. Lee. J. Appl. Phys., **112**, 084318 (2012). DOI: 10.1063/1.4759253
[48] D.E. Steinhauer, C.P. Vlahacos, F.C. Wellstood, S.M. Anlage, C. Canedy, R. Ramesh, A. Stanishevsky, J. Melngailis. Rev. Sci. Instrum., **71**, 2751 (2000). DOI: 10.1063/1.1150687
[49] J.H. Lee, S. Hyun, K. Char. Rev. Sci. Instrum., **72**, 1425 (2001). DOI: 10.1063/1.1342032
[50] K. Lai, W. Kundhikanjana, M. Kelly, Z.X. Shen. Rev. Sci. Instrum., **79**, 063703 (2008). DOI: 10.1063/1.2949109
[51] Z. Wei, Y.-T. Cui, E.Y. Ma, S. Johnston, Y. Yang, R. Chen, M. Kelly, Z.-X. Shen, X. Chen. IEEE Trans. Microwave Theory Tech., **64**, 1402 (2016). DOI: 10.1109/TMTT.2016.2537801